Soil Dynamics and Earthquake Engineering 56 (2014) 28–43

Contents lists available at ScienceDirect

Soil Dynamics and Earthquake Engineering

journal homepage: www.elsevier.com/locate/soildyn

Simplified approximate method for analysis of rocking systems accounting for soil inelasticity and foundation uplifting

I. Anastasopoulos [a,*,1], Th. Kontoroupi [b,1]

[a] Division of Civil Engineering, University of Dundee, United Kingdom
[b] Department of Civil Engineering and Engineering Mechanics, Columbia University, United States

ARTICLE INFO

Article history:
Received 22 October 2012
Received in revised form
25 September 2013
Accepted 1 October 2013

Keywords:
Rocking foundation
Nonlinear analysis
Simplified method
Soil–structure interaction

ABSTRACT

A simplified approximate method to analyze the rocking response of *SDOF* systems lying on compliant soil is introduced, accounting for soil inelasticity and foundation uplifting. The soil–foundation system is replaced by a *nonlinear rotational* spring, accompanied by a linear rotational dashpot, and linear horizontal and vertical springs and dashpots. Considering a square footing on clay under undrained conditions, the necessary moment–rotation (M–θ) relations are computed through *monotonic pushover* finite element (FE) analyses, employing a thoroughly-validated constitutive model. *Cyclic pushover* analyses are performed to compute the damping–rotation (C_R–θ) relations, necessary to calibrate the rotational dashpot, and the settlement–rotation (Δw–θ) relations, required to estimate the dynamic settlement. The effectiveness of the simplified method is verified through *dynamic* time history analyses, comparing its predictions with the results of 3D FE analyses. The simplified method is shown to capture the entire rotation time history $\theta(t)$ with adequate accuracy. The latter is used to compute the time history of dynamic settlement $w(t)$, employing a simplified approximate procedure. The proposed simplified method should, by no means, be considered a substitute for more sophisticated analysis methods. However, despite its limitations, it may be utilized for (at least preliminary) design purposes.

1. Introduction

Soil–foundation–structure interaction (SFSI) has been the object of extensive research over the last decades in an attempt to gain deeper insight into the seismic performance of structures (e.g., [35,59,36,21,57,61,22]). Nevertheless, a principal goal of foundation design, as entrenched in current seismic codes, is to maintain “elastic” soil–foundation response. According to capacity design principles, full mobilization of strength in the foundation is prevented, by guiding failure onto the superstructure (through application of appropriate over-strength factors). Strong earthquakes over the last 20 years, though, have shown that inelastic soil–foundation response may be inevitable. In fact, seismic records from the earthquakes of Northridge (1994) and Kobe (1995) have proved that very high levels of *PGA* and *PGV* can be experienced in near-fault zones. The recent Tohoku (2011) earthquake is another example of dramatically strong recorded *PGA* of up to 3 g [17].

Apparently, under such severe seismic shaking the assumption of elastic soil–foundation response cannot be considered realistic. Yet, it has been suggested by a growing body of researchers that soil–foundation nonlinear response may have a beneficial effect on the superstructure and it should be therefore considered in design (e.g., [50,24,53,18,46,54,32,19,3,2,27,28,38,39]). Nonlinear foundation behavior may involve *sliding* and/or *uplifting* of the foundation from the supporting soil, and/or mobilization of soil bearing capacity. In any of these cases, the finite capacity of the foundation may act as “rocking isolation” [46], limiting the inertia forces transmitted onto the superstructure, thus protecting it against seismic motions exceeding its design. Besides, such a design alternative offers greater safety margins in terms of ductility, since it exploits the inherent ductility associated with progressive soil failure.

To this end, an urgent need is arising to explicitly account for *nonlinear SFSI* and its beneficial effects in modern seismic design. Nonlinear foundation response could be allowed during strong seismic shaking, while ensuring that the developing displacements and rotations will not jeopardize the structural integrity of the superstructure. So far, a substantial amount of research has been conducted, including *experimental* (e.g. [45,18,41,37,9,51,19]) and *analytical* studies: (i) finite element (FE) or boundary element approaches, in which both the structure and the soil are modeled together in one single system through an assemblage of elements (e.g. [11,10,58,44,31,23,30]); (ii) rigorous plasticity-based macro-element formulations (e.g., [49,50,43,13,12,16]); (iii) Winkler-based

* Corresponding author. Tel.: +44 1382 385720; fax: +44 1382 384816.
E-mail addresses: i.anastasopoulos@dundee.ac.uk, ianast@civil.ntua.gr (I. Anastasopoulos).
[1] Formerly National Technical University of Athens, Greece.

0267-7261/$ - see front matter © 2013 Elsevier Ltd. All rights reserved.
http://dx.doi.org/10.1016/j.soildyn.2013.10.001

approaches, where the soil is replaced by a series of distributed nonlinear springs and dashpots (e.g., [33,1,56]); and (iv) simplified approaches, such as the iterative procedure proposed by Paolucci et al. [52] to be incorporated to the Direct Displacement-Based Design (DDBD) method [55].

Nonlinear FE simulation, where both the superstructure and the soil–foundation system are modeled as a whole, is probably one of the best ways to simulate the response of rocking-isolated systems. However, such an approach is not computationally efficient and requires (reasonably) sophisticated and adequately validated constitutive models, rendering its application difficult in everyday engineering practice. Meanwhile, the current state-of-the art in nonlinear analysis of foundations emphasizes the development of macro-element models. According to this approach, the entire soil-foundation system is replaced by a single element, capable of portraying the rocking response in terms of rotation and dynamic settlement. However, the developed macro-element models have not yet been introduced in commercial FE codes and therefore, their use is limited. Moreover, extensive calibration is required in order to produce ready-to-use parameter "libraries" – a major issue that should be addressed in order to encourage their use in practice.

On the other hand, simplified methods that account for *nonlinear SFSI*, such as the procedure proposed by Paolucci et al. [52], may have substantial benefits, including: (i) easy implementation in commercial numerical analysis codes; (ii) limited calibration requirements; and (iii) applicability by non-specialists. Moreover, such simplified consideration of the nonlinear response of the soil-foundation system allows for more detailed and realistic modeling of the superstructure, which is likely to be a key issue in real-life engineering projects. Last but not least, by avoiding complicated 3D FE modeling, great savings in terms of computation time can be achieved. Consequently, the development of simplified approaches to account for *nonlinear SFSI* is of paramount importance in order to facilitate the application of such novel seismic design concepts in engineering practice.

Aiming to overcome the aforementioned barriers concerning the existing more sophisticated methods of analysis (such as macro-elements and 3D FE modeling), and to provide a framework for future research on the subject, this paper introduces a simplified approximate method to simulate the seismic response of a system rocking on compliant soil, accounting for fully inelastic soil response and geometric nonlinearities (such as foundation uplifting and second order effects). To demonstrate its effectiveness, the proposed simplified method is applied to a single degree of freedom (SDOF) system, representative of a bridge pier, comparing the predicted response with the results of more rigorous 3D FE analyses. The introduced simplified analysis method should, by no means, be viewed as capable of reproducing all aspects of complex soil response, or as a substitute of more elaborate methods. However, despite its limitations, it may be utilized for (at least preliminary) design purposes.

2. Problem definition and outline of the simplified method

As shown in Fig. 1a, the investigated problem refers to a SDOF system of height h carrying concentrated mass m, lying on a square surface foundation of width B on a clay stratum of depth z, undrained shear strength S_u, shear wave velocity V_s, and density ρ. To focus on the nonlinear response of the foundation, the oscillator is assumed practically rigid. Inspired by the simplified procedure proposed by Paolucci et al. [52], a simplified method is introduced to account for *nonlinear SFSI* effects. As illustrated in Fig. 1b, the soil-foundation system is replaced by springs and dashpots (in parallel). Since the considered problem is rocking-dominated, the horizontal (K_H and C_H) and vertical (K_V and C_V) springs and dashpots can be assumed elastic, and published solutions are directly applicable (e.g., [21]). As shown by Gajan and Kutter [20], the response is rocking-dominated when $h/B>1$. In such a case, the cyclic rotation is much larger than the normalized cyclic sliding displacement, irrespective of the factor of safety F_S. Hence, the nonlinearities related to sliding can be ignored, which means that the related horizontal springs and dashpots can be reasonably approximated as elastic.

With respect to the rotational degree of freedom, instead of using an equivalent linear rotational spring, requiring an iterative procedure to capture the nonlinear response of the soil-foundation system (as in [52]), the proposed simplified method employs a *nonlinear rotational spring* accompanied by a *linear dashpot*, the properties of which are estimated through nonlinear 3D FE analyses. After the necessary calibration, the proposed procedure can be quite straightforward, not requiring iterations to compute

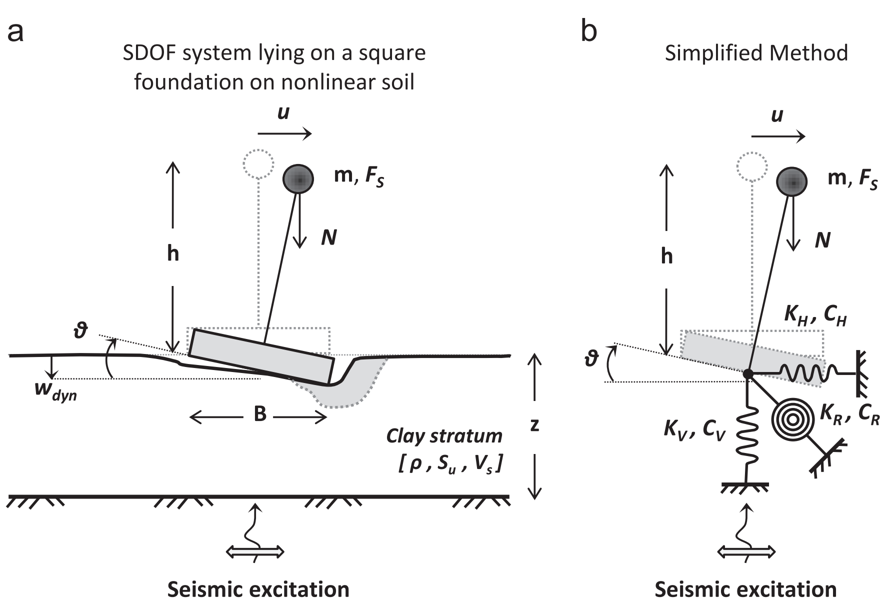

Fig. 1. Problem definition: (a) SDOF system lying on a square surface foundation on a homogeneous clay stratum; and (b) proposed simplified method where the soil–foundation system is replaced by a *nonlinear* rotational spring K_R, accompanied by a linear dashpot C_R, as well as linear vertical and horizontal springs and dashpots, K_V and C_V , and K_H and C_H, respectively.

the response of the rocking foundation–structure system. Since such elements can be easily introduced in commercial FE codes, capable of performing dynamic time history analyses, the proposed methodology can be easily applicable in practice, without requiring calibration of sophisticated models and avoiding the need for time consuming 3D FE analyses. As it will be shown later on, the proposed method may capture with adequate accuracy the entire rotation time history $\theta(t)$. The latter is used to compute the time history of dynamic settlement $w(t)$, employing a simplified approximate procedure, also based on FE analysis results. A similar procedure had been earlier postulated by Kutter et al. [42] and Deng et al. [14], who suggested that the settlement can be correlated with the rotation time history $\theta(t)$.

In order to implement the proposed method, three relations are required, all of them being a function of the factor of safety against vertical loads $F_S = N_{uo}/N$, where N_{uo} is the bearing capacity of the footing under purely vertical loading, and $N = mg$ is the vertical load due to the mass of the superstructure (assuming that the footing is massless): (a) the moment–rotation (M–θ) relation, required to define the *nonlinear* rotational spring K_R; (b) the damping coefficient–rotation (C_R–θ) relation, required to define the rotational dashpot C_R; and (c) the dynamic settlement–rotation (Δw_{dyn}–θ) relation, required to compute the settlement. The three necessary relations are computed employing the FE method, applying a thoroughly validated soil constitutive model [4], and focusing on square shallow foundations. The same methodology can be employed for other footing shapes (rectangular, circular, strip), or for embedded foundations (see also [25]). Alternatively, the required relations can be produced *experimentally*, on the basis of cyclic pushover tests (e.g., [40,18,5]). Thus, the practicing engineer may directly apply the proposed methodology utilizing the provided FE-derived relations, or select from the literature other relations that may be considered more appropriate.

The vertical component of the seismic motion has not been included in the analyses, and its effect on settlement accumulation cannot be addressed through the presented simplified method. Although this is clearly a limitation of the proposed simplified analysis method, it is not expected to have an appreciable effect on the response, at least as far as the natural vertical component of the earthquake is concerned. The latter is typically of much higher frequency and not correlated to the horizontal component. Its effect has been shown to be of minimal importance in Kourkoulis et al. [39], using a 2-storey rocking-isolated frame structure as an example. However, a valley-generated parasitic vertical component *can be detrimental for overlying structures*, and its effect should be taken into account. In contrast to the natural vertical component, being a direct result of geometry, it is fully correlated and of practically the same dominant period with the horizontal component [26], and can therefore have a detrimental effect on system performance and the accumulated settlements.

3. Numerical analysis methodology

The three necessary relations (M–θ, C_R–θ, and Δw–θ) are derived through 3D FE analysis of the foundation–structure system. The M–θ relations are computed on the basis of displacement-controlled *monotonic* pushover analyses; *cyclic* pushover analyses are conducted to derive the C_R–θ and Δw–θ relations. Then, the seismic performance of the rocking system is computed through *dynamic* time history analysis: (a) employing the 3D FE model of the soil–foundation–structure system; and (b) applying the proposed simplified method. The results of the two approaches are compared to verify the effectiveness of the simplified method, and to derive insights on the main factors affecting the response.

The 3D FE model (Fig. 1a) comprises the entire soil–foundation–structure system, taking account of material (soil) and geometric nonlinearities (uplifting and P–Δ effects). As illustrated in Fig. 2, taking advantage of problem symmetry (since rotation on a single plane is studied), only half of the *soil–foundation–structure* system is modeled to reduce the computational cost. The bridge pier is modeled with elastic beam elements, while the deck is represented by a concentrated mass element. As previously mentioned, to focus on foundation performance, the oscillator is assumed practically rigid. The footing is modeled with elastic (8-node) continuum elements, and is assumed massless. The soil, consisting of an idealized homogeneous clay stratum, is also modeled with continuum elements, but is of course nonlinear. Special contact elements are introduced at the soil–foundation interface, permitting detachment from the supporting soil. *"Free-field*" boundaries are used at the two lateral (normal to the rotation plane) boundaries of the model. However, as discussed in detail in Kourkoulis et al. [38], even elementary boundaries placed at an adequately large distance from the footing would be sufficient for such rocking-dominated problems.

Soil behavior is modeled through a nonlinear kinematic hardening model, with a Von Mises failure criterion and associated flow rule [4]. The evolution law of the model consists of a nonlinear kinematic hardening component, which describes the translation of the yield surface in the stress space, and an isotropic hardening component, which defines the size of the yield surface as a function of plastic deformation (see also [29]). Calibration of model parameters requires knowledge of: (a) the undrained shear strength S_u; (b) the small-strain stiffness (expressed through G_o or V_s); and (c) the stiffness degradation (G–γ and ξ–γ curves). More details on the model, as well as model calibration and comparisons of model predictions in terms of G–γ and ξ–γ curves against experimental results can be found in [4].

In the case of the simplified approach (Fig. 1b), the superstructure is modeled using exactly the same model, but the soil–foundation system is replaced by linear horizontal (K_H and C_H) and vertical (K_V and C_V) springs and dashpots, a nonlinear rotational spring K_R, and a linear rotational dashpot C_R. While K_H, K_V, C_H, and C_V are calibrated on the basis of published solutions [21], the derived M–θ and C_R–θ relations are used for K_R and C_R. The simplified model is subjected to dynamic time history analysis, employing as seismic excitation the acceleration time history at the ground surface. Based on the computed rotation time history $\theta(t)$,

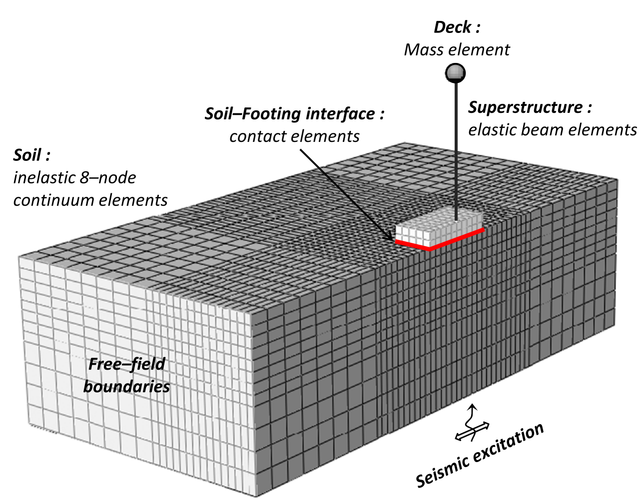

Fig. 2. Rigorous 3D finite element model comprising the entire soil–foundation–structure system, taking account of material (soil) and geometric nonlinearities (uplifting and P–Δ effects). Taking advantage of problem symmetry, only half of the model is analyzed.

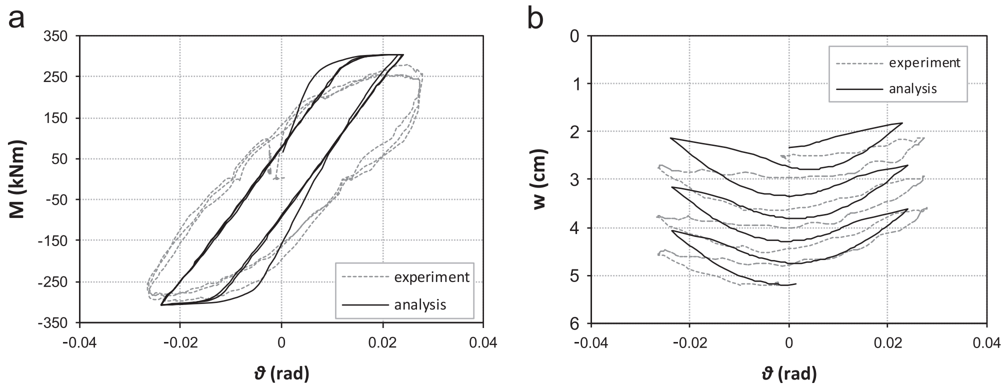

Fig. 3. Model validation against UC Davis centrifuge model tests [40] – cyclic pushover of a rectangular footing of static safety factor $F_S=2.6$, resting on remolded San Francisco Bay mud (second loading packet). Comparison of numerical prediction with experimental measurement: (a) moment–rotation (M–θ), and (b) settlement–rotation (w–θ) response.

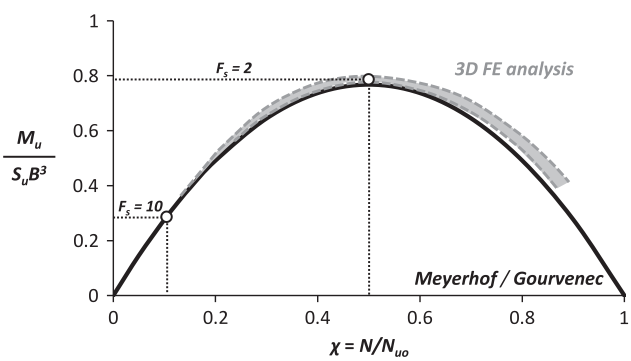

Fig. 4. Comparison of FE analysis results with published failure envelopes [47,30] for various B/L ratios: normalized moment capacity M_u/S_uB^3 with respect to normalized vertical load $\chi=N/N_{uo}$ $(=1/F_S)$.

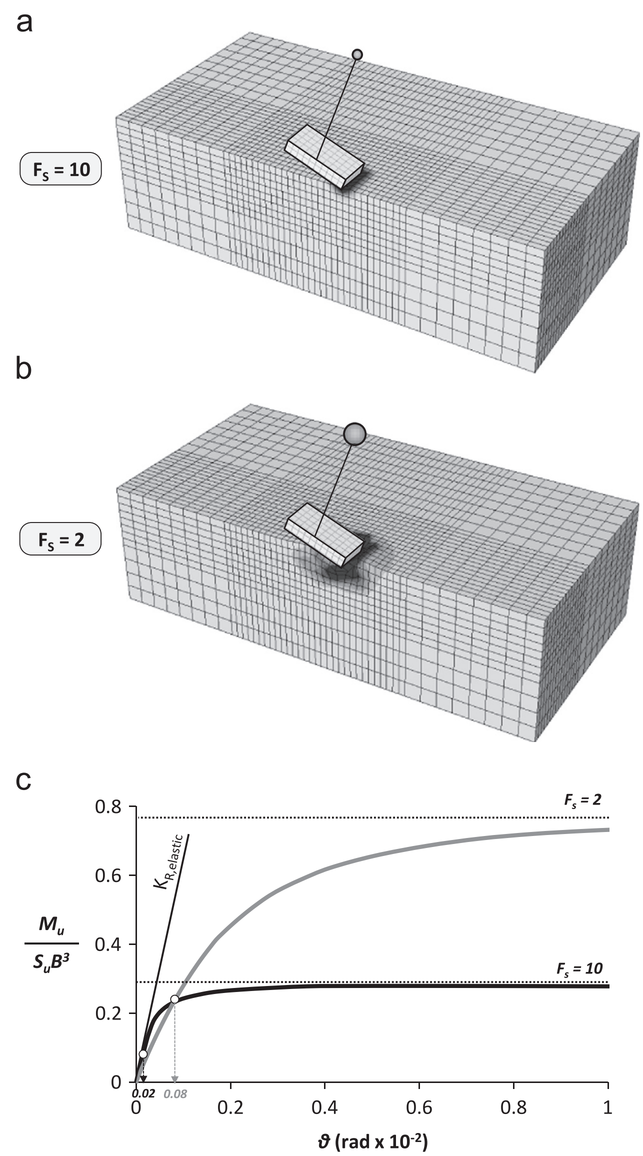

Fig. 5. Square shallow footing subjected to monotonic pushover loading. Snapshots of deformed mesh with superimposed plastic strain contours for: (a) $F_s=10$, and (b) $F_s=2$; (c) moment–rotation (M–θ) response for $F_s=10$ and 2.

and the derived Δw–θ relations, a simplified procedure is employed to compute the settlement time history $w(t)$.

3.1. Model validation

The 3D FE modeling technique has been validated against UC Davis centrifuge model tests [40,18] and large-scale tests [15,48], as discussed in Anastasopoulos et al. [4], but also against reduced-scale tests conducted at the Laboratory of Soil Mechanics of the National Technical University of Athens [6]. One such comparison is reproduced in Fig. 3, referring to a rectangular foundation with $F_S=2.6$, resting on remolded San Francisco Bay mud. Conducted at $n=20$ g, cyclic loading was applied in packets of increasing amplitude. The second of those packets is illustrated herein, having maximum rotation amplitude $\theta_{max}\approx 0.03$ rad. The model prediction is adequately accurate both in terms of footing moment capacity $M_{ult}\approx 300$ kNm (Fig. 3a), and with respect to the accumulated settlement (Fig. 3b). The M–θ loops reveal strongly nonlinear response, accompanied by substantial soil plastification. The analysis seems to under-predict energy dissipation, something that is probably associated with an under-prediction of foundation uplifting. Still though, the accumulation of settlement is predicted with remarkable accuracy.

The model is further validated herein against published failure envelopes for surface foundations subjected to combined M–Q–N loading [11,30]. One such comparison against the failure envelopes of Gourvenec [30] is portrayed in Fig. 4, referring to an $h/B=2$ *SDOF* system lying on shallow footings of various shapes (strip $B/L=0$; square $B/L=1$; rectangular $B/L=3$; and circular, where B refers to the width of the side normal to the axis of rotation) ignoring P–Δ effects (to produce compatible results). The plot presents the normalized foundation moment capacity M_u/S_uB^3 as a function of the normalized vertical load $\chi=N/N_{uo}=1/F_S$ (where N_{uo} is the bearing capacity under purely vertical loading). The numerical prediction compares well with the classic solution of Meyerhof [47], overestimating M_u/S_uB^3 by about 10% for $\chi > 0.3$ (i.e., for $F_S < 3$). Ignoring P–Δ effects, the moment capacity of the foundation is maximized for a critical value of the safety factor against vertical loads $F_S = 2$ ($\chi = 0.5$).

Admittedly, the model employed herein has not yet been validated for all possible combinations of moment to shear ratio, embedment depth, and footing shape. While there is a breadth of failure envelopes in the literature, the experimental data dealing with cyclic or dynamic loading are much more limited. Specific cases have been tested experimentally, and only these can and have been used for validation as summarized in Anastasopoulos et al. [7].

4. Moment–rotation relations

The M–θ relations are computed through displacement-controlled monotonic pushover analyses, utilizing the previously presented 3D FE model. To derive results of generalized applicability, the analysis is conducted following the dimensional formulation presented in Kourkoulis et al. [38]. The FE analyses are conducted for different factors of safety against vertical loading $F_S = 2$, 2.5, 3.3, 5, and 10 (corresponding to $\chi = N/N_{uo} = 0.5$, 0.4, 0.3, 0.2, and 0.1). Static factors of safety $F_S < 2$ are rarely applied in practice (to limit settlement), and are therefore not considered herein. On the other hand, for $F_S > 10$ the rocking response is almost purely uplifting-dominated, with soil inelasticity playing only a minor role. For the case of clay, this has been shown in Gazetas et al. (2013). In the case of sand, soil nonlinearity may be important even for much larger F_S. All of the results presented herein refer to a relatively slender system, having a slenderness ratio $h/B = 2$ (corresponding to a slenderness ratio $H/B = 4$ of the equivalent rigid block, where $H = 2h$).

Example analysis results are depicted in Fig. 5, comparing the monotonic pushover response of a (very) lightly-loaded ($F_S = 10$) to that of a heavily-loaded ($F_S = 2$) footing. As revealed by the snapshots of deformed mesh with superimposed plastic strain contours, while the response of the lightly-loaded footing is clearly uplifting-dominated (Fig. 5a), substantial soil yielding is observed in the case of the heavily-loaded (Fig. 5b). In other words, the decrease of F_S tends to diminish the extent of uplifting, leading to an increase of soil plastification at the same time. The moment–rotation (M–θ) response of the two footings is compared in Fig. 5c. In accord with the failure envelopes of Fig. 4, the moment capacity of the heavily-loaded footing is substantially larger than that of the lightly-loaded. Exactly the opposite is observed in terms of the initial (i.e., for $\theta \to 0$) rotational stiffness $K_{R,0}$, with the lightly-loaded footing being substantially stiffer.

To define the necessary relations, the M–θ response is divided in three characteristic phases, which are described in detail in the next sections: (a) quasi-elastic response (for very small rotation $\theta \to 0$); (b) plastic response (referring to the ultimate capacity, for large rotation θ); and (c) nonlinear response (which is the intermediate stage between the quasi-elastic and the plastic phases).

4.1. Quasi-elastic response

The first phase of response refers to very small rotation θ. The effective (secant) rotational stiffness is a function of θ and F_S: $K_R = f(\theta, F_S)$. For a given factor of safety F_S, the initial (i.e., for $\theta \to 0$) rotational stiffness can be defined as

$$K_{R,0} = K_R(0, F_S) \tag{1}$$

As shown in Fig. 5c, for the lightly-loaded ($F_S = 10$) footing, $K_{R,0}$ is very close to the purely elastic rotational stiffness [21]:

$$K_{R,elastic} = 3.65 \frac{Gb^3}{1-\nu} \tag{2}$$

where $b = B/2$, G is the small strain shear modulus of soil, and ν the Poisson's ratio. Since the rocking mechanism is quite shallow, estimating G as the average shear modulus to a depth equal to the width B of the foundation is considered as a reasonable approximation. In fact, this has been indirectly confirmed by the reduced-scale experiments reported in Anastasopoulos et al. [5,6], where it was shown that the soil properties at depth larger than B are not affecting the rocking response. In stark contrast, a substantial difference is observed for the heavily-loaded ($F_S = 2$) footing. This reduction of $K_{R,0}$ is directly related to the initial soil yielding due to the imposed vertical load N (before application of moment loading). In other words, even before the lateral loading is applied, the soil underneath the foundation behaves in a nonlinear manner, and this affects the initial value of the rotational stiffness $K_{R,0}$. Based on the 3D FE analysis results, $K_{R,0}$ can be (approximately) expressed as

$$K_{R,0} = K_{R,elastic}\left(1 - 0.8\frac{1}{F_S}\right) \tag{3}$$

The 0.8 parameter in the above equation has been “fitted” to analysis results and can be claimed to be valid for $F_S \geq 1.1$. Given that the latter refer to clay, the specific parameter will not be applicable to sand. Still though, Eq. (3) is not expected to be different in qualitative terms. This will be covered in a forthcoming publication, based on recently conducted reduced-scale experiments of rocking foundations lying on sand.

4.2. Plastic response

This phase refers to the ultimate capacity of the footing, and is quite straight-forward to define on the basis of the previously discussed failure envelopes. As thoroughly discussed in Gazetas et al. [25], the failure envelope can be defined as follows (see also Fig. 4):

$$\frac{M_u}{N_u B} = 0.55\left(1 - \frac{N_u}{N_{uo}}\right) \tag{4}$$

where N_{uo} is the bearing capacity for purely vertical loading [47,30]:

$$N_{uo} \approx (\pi + 3) S_u B^3 \tag{5}$$

The above expression (Eq. (4)) exceeds by just 10% the classical solution of Meyerhof [47], the failure envelopes of Gourvenec [30], and to what is suggested by Deng et al. [14]. Observe that the maximum moment capacity $M_u \approx 0.138 N_u B$ is attained for $N_u/N_{uo} = 0.5$ (or $F_s = 2$), being just a little higher than the classic value $M_u = 0.125 N_{uo}$.

4.3. Nonlinear response

This corresponds to the intermediate phase, bridging the gap between the quasi-elastic and plastic response. If the soil behaved as an ideally elastic–plastic material, there would be no need to consider this intermediate phase of response, and the previously described solutions would be enough to completely define the necessary M–θ relations. However, as revealed by Fig. 5c, the soil–foundation system exhibits strongly nonlinear response long before reaching its ultimate capacity. Hence, there is a need for a “connection” between the quasi-elastic and the plastic part of the M–θ relations. This is performed on the basis of 3D FE analysis results, following the dimensional formulation presented in Kourkoulis et al. [38] and Gazetas et al. [25].

As shown in Fig. 5c, the initiation of the nonlinear phase is a function of F_s. While the lightly-loaded ($F_s = 10$) footing starts exhibiting nonlinear response for $\theta \approx 0.02 \times 10^{-2}$ rad, in the case of the heavily-loaded ($F_s = 2$) nonlinearity becomes observable much later, for $\theta \approx 0.08 \times 10^{-2}$ rad. This difference is due to the vertical load N acting on the foundation, the increase of which tends to hinder separation and uplifting. In the absence of soil nonlinearity, considering a footing (of any shape) rocking on elastic half-space, the overturning moment to initiate uplifting (i.e., the contact stresses at the edge of the footing are reduced to zero) would be [8]:

$$M_{uplift} \approx \frac{NB}{4} \tag{6}$$

where B is the width of the footing in the direction of rocking. Therefore, the uplifting rotation θ_{uplift} can be defined as

$$\theta_{uplift} \approx \frac{N\,B}{4\,K_{R,\ elastic}} \tag{7}$$

As previously discussed, the initial quasi-elastic rotational stiffness $K_{R,0}$ decreases with the decrease of F_s due to the increasingly important initial soil yielding (due to the vertical load N, before application of moment loading). Therefore, when considering soil inelasticity it is reasonable to assume that the equivalent "uplifting" rotation will be a function of $K_{R,0}$ rather than $K_{R,elastic}$. Hence, combining Eqs. (3) and (7), a characteristic rotation θ_S is defined:

$$\theta_S \approx \frac{NB}{4K_{R,0}} = \frac{NB}{4K_{R,elastic}\left(1-0.8\frac{1}{F_S}\right)} \tag{8}$$

As shown in Fig. 6a, θ_S can be used to normalize the rotation θ, allowing the expression of the M–θ relations in non-dimensional form: $M/S_uB^3 = f\,(\theta/\theta_S)$. Thanks to the normalization of θ with θ_S, the shape of the *moment–rotation* curves is almost identical for all cases examined, irrespective of F_S. Hence, if we normalize M/S_uB^3 with the moment capacity M_u/S_uB^3 of each curve, the *moment–rotation* curves of Fig. 6a "collapse" in the single non-dimensional curve of Fig. 6b. The latter is simplified further, being approximated by piecewise linear segments. The resulting non-dimensional M–θ relation encompasses: (a) a quasi-elastic branch, for $\theta/\theta_s \leq 1/3$; (b) a plastic branch, for $\theta/\theta_s > 10$; and (c) an intermediate nonlinear branch, for $1/3 < \theta/\theta_s \leq 10$, consisting of four segments, as illustrated in Fig. 6b.

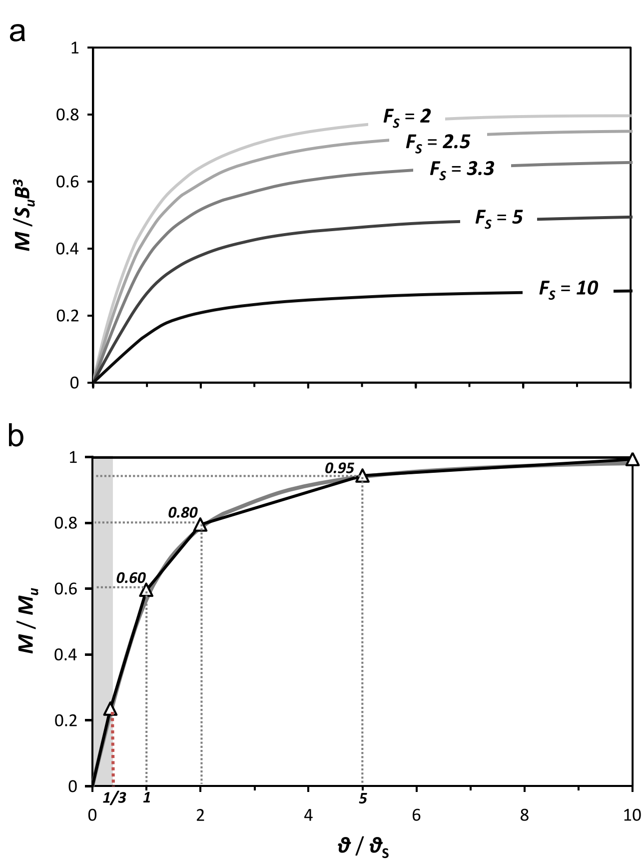

Fig. 6. (a) Normalized moment–rotation response for different factors of safety against vertical loading F_S; and (b) non-dimensional unique moment–rotation (M–θ) relation and simplified piecewise approximation.

5. Damping–rotation relations

For the rocking-dominated systems considered herein, the damping comprises three different components: (a) radiation damping, (b) hysteretic damping, and (c) damping due to impacts. In the idealized case of elastic soil response (without uplifting or soil inelasticity), radiation is the main source of damping: waves emanating from the dynamically oscillating foundation disperse to infinity, "absorbing" energy from the rocking system [21]. However, when considering strongly inelastic response due to material (soil) and geometric nonlinearities (uplifting), radiation damping is practically negligible compared to hysteretic damping. Under strong seismic shaking, which is the main target of the proposed simplified method, the fundamental period T_{soil} of the soil layer will be significantly lower than both the predominant period T_p of the earthquake and the natural period T_n of the rocking system – especially in view of the fact that the latter increases substantially due to uplifting. It is noted that such period elongation is not a special attribute of rocking systems, but is the rule for any nonlinear system. As a result, the system will respond below its "cutoff" frequency (i.e., the frequency below which radiation damping is not significant, see [21]), and radiation damping will be of the order of 1% to 2%. Damping due to impacts is also considered negligible compared to hysteretic damping, being important only when soil inelasticity is limited.

Based on the above, emphasis is placed on the hysteretic component of rotational damping. The latter is computed on the basis of displacement-controlled cyclic pushover analyses, utilizing the 3D FE model. The FE analyses are conducted for the previously discussed factors of safety against vertical loading F_S=2, 2.5, 3.3, 5, and 10. The rotational damping coefficient for the simplified SDOF model is assumed to be a function of the effective (secant) rotational stiffness K_R, the hysteretic damping ratio ξ, and a characteristic frequency ω:

$$C_R \approx \frac{2\,K_R\xi}{\omega} \tag{9}$$

while the effective (secant) stiffness K_R is computed utilizing the previously discussed M–θ relations, the hysteretic damping ratio ξ is computed through the M–θ loops of the cyclic pushover analyses. For this purpose, the SDOF is subjected to cyclic rotation of increasing amplitude. The hysteretic damping ratio ξ is calculated according to its standard definition:

$$\xi \approx \frac{\Delta E/E}{4\pi} \tag{10}$$

where ΔE is the area of the M–θ loops, representing the energy consumed during one cycle of loading, and E is the corresponding elastic energy. As discussed below, the selection of the characteristic frequency ω is not that straightforward.

The results of the analyses are summarized in Fig. 7a, where the hysteretic damping ratio ξ is plotted as a function of the dimensionless cyclic rotation amplitude θ/θ_S and the factor of safety against vertical loading F_S. As expected, ξ increases with the decrease of F_S, since energy dissipation increases with soil nonlinearity (the area enclosed by the M–θ loops becomes larger). Exactly for the same reason, ξ is an increasing function of θ/θ_S. Exactly the opposite is observed for the normalized effective (secant) rotational stiffness $K_R/K_{R,elastic}$, which (as also expected)

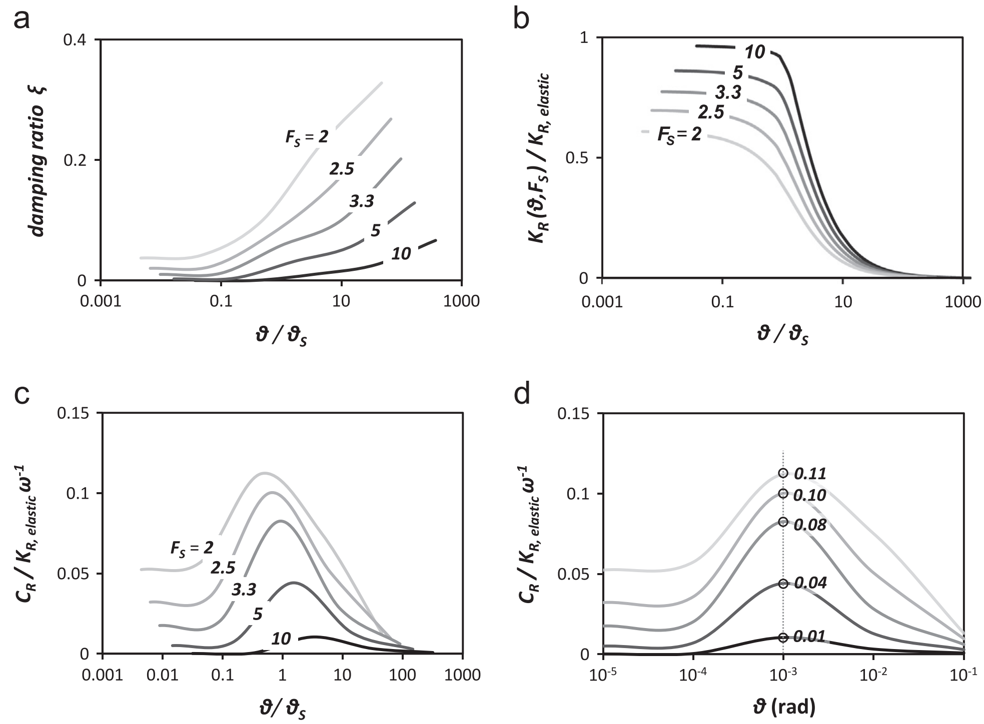

Fig. 7. (a) Damping ratio ξ with respect to the dimensionless rotation θ/θ_S and factor of safety against vertical loading F_s; (b) normalized rotational stiffness $K_R(\theta,F_S)/K_{R,elastic}$ with respect to θ/θ_S and F_s; (c) dimensionless damping coefficient $CR/K_{R,elastic}\omega^{-1}$ with respect to θ/θ_S and Fs ; and (d) $CR/K_{R,elastic}\omega^{-1}$ with respect to θ and F_s.

increases with F_S, while being a decreasing function of θ/θ_S (Fig. 7b): the increase of soil inelasticity leads to a decrease of the secant stiffness. As a result, being the product of K_R and ξ (Eq. (10)) the damping coefficient C_R is not that sensitive to θ/θ_S (assuming a constant value of ω). As shown in Fig. 7c, the normalized damping coefficient $C_R/K_{R,elastic}\omega^{-1}$ plotted with respect to θ/θ_S is a "bell shaped" curve, with its maximum at $\theta/\theta_S \approx 1$. Interestingly, if we plot $C_R/K_{R,elastic}\omega^{-1}$ as a function of the absolute value of θ (Fig. 7d), the maximum is observed for roughly 10^{-3} rad, for all cases examined. The value of the maximum $C_R/K_{R,elastic}\omega^{-1}$ increases with the decrease of F_S.

As revealed by the derived C_R–θ relations, a nonlinear dashpot would ideally be required. Nevertheless, since most commercial FE codes accept a single value of C_R, a simplifying approximation is proposed in order to maintain simplicity. As discussed below, the numerical prediction using the simplified model compares well with the results of the more rigorous 3D FE model, when the maximum value of the normalized C_R–θ curve is adopted. Therefore, in terms of a reasonable simplifying assumption, it is recommended to directly use this value to compute the necessary C_R as a function of F_S only, as indicated in Fig. 7d. In case another value of F_S is to be studied (not included herein), the normalized damping coefficient may be obtained through linear interpolation (an acceptable simplification, given all of the above simplifying assumptions).

As previously discussed, the absolute value of C_R also depends on the angular frequency $\omega=2\pi/T$. The latter is also a function of rotation, as the effective period T_n of the rocking system increases with θ/θ_S [25]. In order to maintain simplicity, a single value of T_n is needed to compute the absolute value of C_R. Based on comparisons between the simplified method and the 3D FE model (to be discussed later on), it is considered as a reasonable simplification to use the initial natural period $T_{n,0}$ of the rocking system (for $\theta/\theta_S=0$). At this point, it should be noted that, although the system is subjected to forced oscillation, the corresponding value of C_R is not related to the predominant period of the excitation T_p. It appears that the initial natural period $T_{n,0}$ is quite dominant, at least for the slender systems considered herein (of relatively large h/b). Within this realm, considering a rigid oscillator (in essence, an inverted pendulum [34]) and assuming that the horizontal displacement is negligible compared to the rocking mode, the initial rocking period (for $\theta/\theta_S=0$) can be written as

$$T_{n,0} = 2\pi\sqrt{\frac{mh^2}{K_{R,0}-mgh}} = 2\pi\sqrt{\frac{mh^2}{K_{R,elastic}\left(1-0.8\frac{1}{F_S}\right)-mgh}} \tag{11}$$

In the case of rocking-isolated systems, such as those considered herein, the fixed-base fundamental period of the superstructure is typically much lower than that of the rocking system: as soon as the foundation starts uplifting, the effective period increases almost exponentially with θ (e.g., [25]). Hence, at least for the systems considered herein, the assumption of a rigid oscillator is not far from reality. As it has been shown in previous studies (e.g., [3,27]), for rocking-isolated systems the drift due to the flexural deformation of the superstructure is negligible compared to the rotational drift (i.e., the drift due to foundation rotation). Hence, the efficacy of the method in terms of prediction of the drift shall not be challenged by the flexibility of the oscillator. Naturally, this will not be the case for conventionally-designed systems, in which case the flexural drift will be much larger than the rotational. In such a case, the response of the foundation will be quasi-elastic, its moment capacity will not be mobilized, and simpler elastic methods are directly applicable.

6. Settlement–rotation relations

The cyclic settlement is computed through displacement-controlled cyclic pushover analyses, utilizing the more rigorous 3D FE model. The FE analyses are conducted for the previously discussed factors of safety against vertical loading F_S=2, 2.5, 3.3, 5, and 10. As for the damping–rotation relations, the system is subjected to cyclic loading of increasing amplitude. Example analysis results are presented in Fig. 8a for a square footing of $F_S=2$. For each cycle of loading, the cyclic settlement Δw (due to one complete loading cycle) is computed, as schematically illustrated in Fig. 8b. The same procedure is applied for all the other factors of safety F_S. A similar correlation of Δw with cyclic rotation θ has been earlier suggested by Gajan et al. [18] on the basis of experimental results of shallow foundations lying on sand.

The resulting settlement–rotation relations are summarized in Fig. 9, referring to the settlement Δw normalized with B, with respect to the rotation θ and the factor of safety against vertical loading F_S. In contrast to the previously discussed M–θ and C_R–θ relations, where the normalization of θ with θ_S had certain advantages, the settlement–rotation relations are more convenient when plotted with respect to the absolute value of θ, as they are almost linear (with the exception of small values of θ). This allows their approximation with a simplified linear expression, as shown

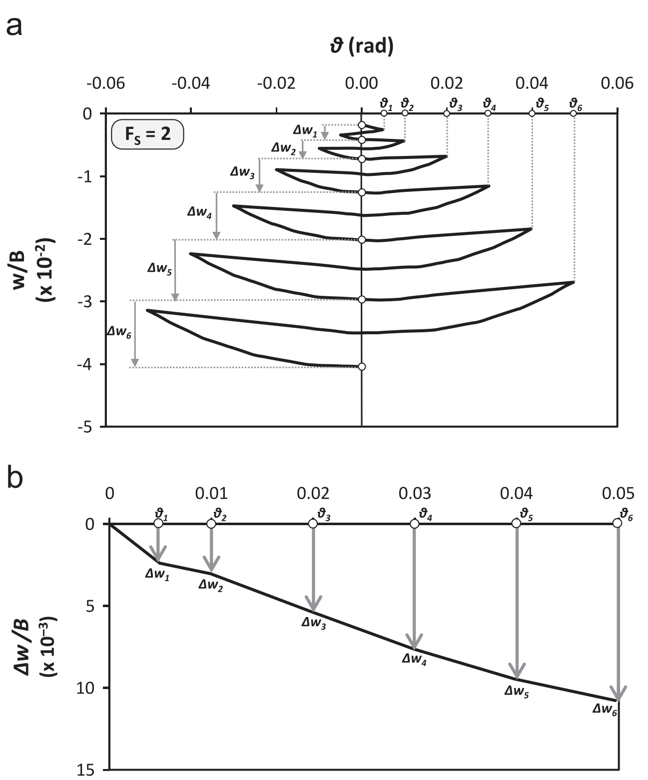

Fig. 8. Example cyclic pushover loading results for a square footing with $F_S=2$: (a) normalized settlement–rotation (w/B–θ) response; and (b) resulting cyclic settlement–rotation relation.

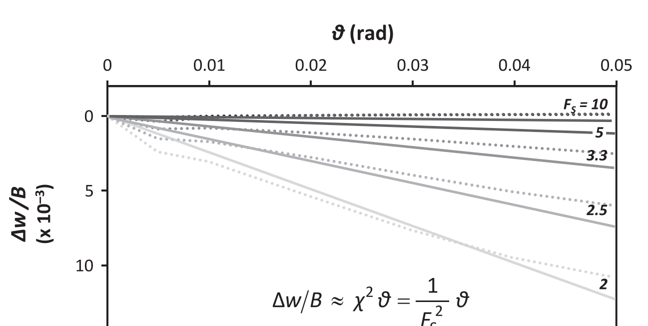

Fig. 9. Simplified cyclic settlement–rotation ($\Delta w/B$–θ) relations for various factors of safety against vertical loading F_S (dotted lines) compared to the simplified linear approximation (continuous lines).

in Fig. 9:

$$\Delta w/B \approx \chi^2|\theta| = \frac{1}{F_S^2}|\theta| \tag{12}$$

It should be noted that the optimum "fit" of FE analysis results is obtained with an exponent of 2.2 (instead of 2) in Eq. (12). However, given the approximate nature of the proposed procedure, the above simplified expression is considered preferable and conservative (especially for large values of F_S). As previously discussed for Eq. (3), the specific parameters have been computed for clay and cannot be directly applicable to sand. Quite interestingly, the range of values predicted by Eq. (12) compares qualitatively well with the experimental results of Gajan et al. [18], which refer to shallow foundations lying on sand. According to the latter, for $\theta \approx 0.05$ rad the dimensionless cyclic settlement $\Delta w/B$ ranges from 0.002 for $F_S > 7$ to roughly 0.01 for $2 < F_S \leq 3.5$.

The simplified procedure to compute the dynamic settlement time history $w/B(t)$ is outlined in Fig. 10 through an illustrative example, referring to a square footing of $F_S=2.5$ subjected to seismic shaking with the Sakarya record. Fig. 10a compares the numerical prediction of the simplified method to the 3D FE analysis. As discussed in more detail in the ensuing, the proposed simplified model captures the rotation time history with quite reasonable accuracy (especially taking account of the various simplifying assumptions it entails). As sketched in Fig. 10b, the computed rotation time history $\theta(t)$ is used to directly compute the settlement time history $w/B(t)$, according to the following procedure:

(a) The computed (using the simplified model) rotation time history $\theta(t)$ is split into a finite number of half-cycles ($\theta_1 \ldots \theta_6$ for the example time window shown herein);
(b) For every half-cycle of amplitude θ, the cyclic settlement is computed using the previously derived settlement–rotation relations. It is assumed that each half-cycle produces (approximately) half the cyclic settlement that is computed using Eq. (12) (which corresponds to a compete cycle of rotation): i.e., a half-cycle of amplitude θ_1 is assumed to generate dynamic settlement $\Delta w_1=\chi^2\theta_1/2$;
(c) The settlement time history is put together by assuming that each half-cycle settlement lasts as much as the corresponding rotation half-cycle (definitely, a reasonable assumption). For example, the first half-cycle settlement Δw_1 is assumed to last t_1, i.e., as much as the first half-cycle of rotation θ_1. Each half-cycle settlement is added to the previous one, leading to the assembly of the entire time history of settlement (presented herein in normalized form).

Apparently, such simplified calculation can only provide an estimate of the accumulated settlement *at the end* of each loading half-cycle. Obviously, the uplifting-generated upward movement of the foundation *during* a rotation half-cycle cannot possibly be captured.

7. Effectiveness of the simplified method

In order to demonstrate the effectiveness of the proposed simplified method, this section compares the numerical prediction of the simplified model with the results of nonlinear dynamic time history analysis using the more rigorous 3D FE model. The analyses are conducted considering a specific SDOF system of height $h=4$ m and $B=2$ m, lying on stiff (over-consolidated) clay of undrained shear strength $S_u=150$ kPa. The comparison is performed for different factors of safety against vertical loading F_S=2, 2.5, 3.3, and 5.

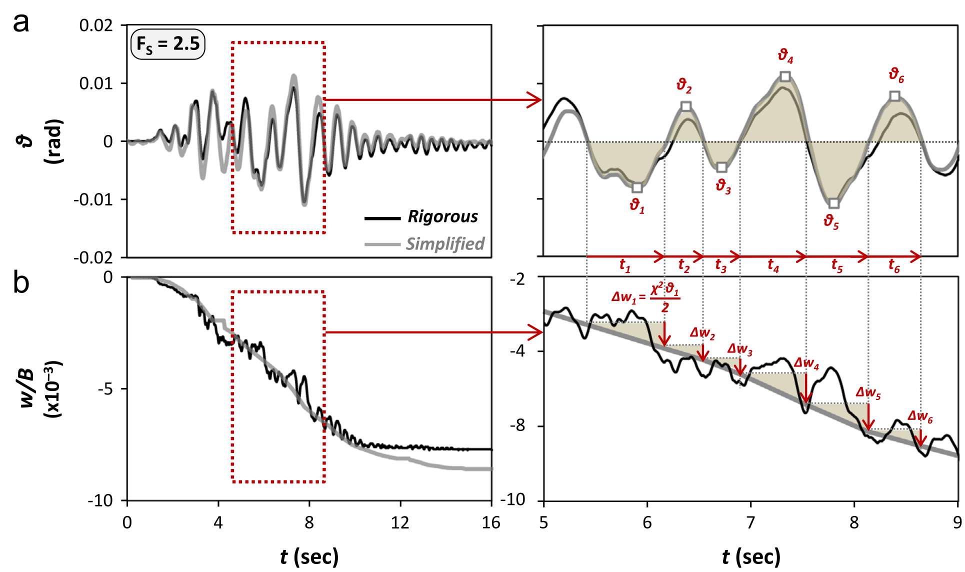

Fig. 10. Example calculation of dynamic settlement time history $w/B(t)$ for a square footing having $F_S=2.5$ subjected to seismic shaking with the Sakarya record: (a) comparison of numerical prediction using the simplified method to the rigorous 3D FE analysis; and (b) illustration of the simplified procedure, where the time history of dynamic settlement is computed directly through the computed rotation time history, making use of the cyclic settlement–rotation relations.

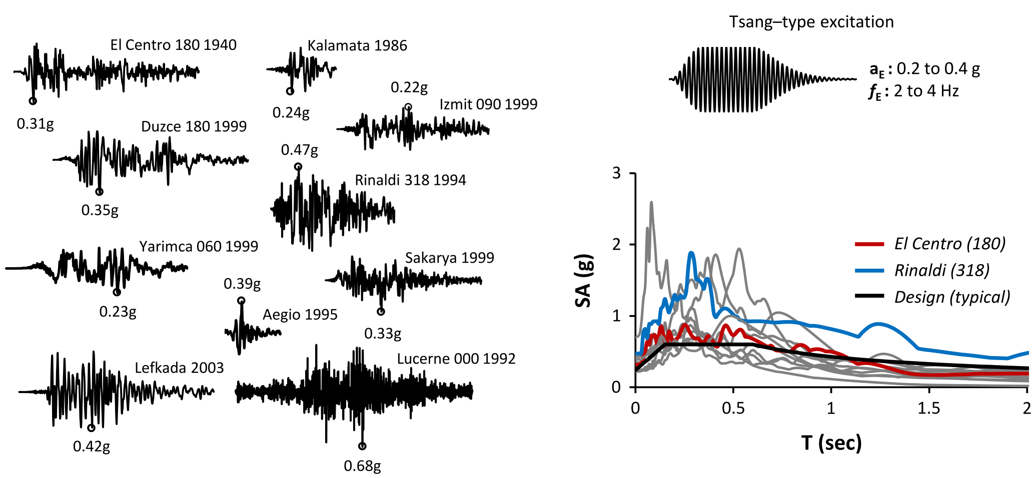

Fig. 11. Artificial Tsang-type motions and real records utilized as seismic excitations for the dynamic time history analyses, along with their acceleration response spectra.

As previously mentioned, apart from the nonlinear rotational spring and the accompanying linear rotational dashpot, the simplified model also requires horizontal (K_H and C_H) and vertical (K_V and C_V) springs and dashpots. For the rocking-dominated problem studied herein, the latter can be assumed linear elastic, and computed by directly applying published solutions [21]:

$$K_V = \frac{4.54Gb}{1-v}, \quad K_H = \frac{9Gb}{2-v} \tag{13}$$

$$C_V = \frac{2K_V\xi}{\omega}, \quad C_H = \frac{2K_H\xi}{\omega}, \tag{14}$$

with respect to K_H and K_V (Eq. (13)), the initial small strain shear modulus G has been assumed. In the latter (Eq. (14)), ξ is assumed equal to 0.05 and $\omega=2\pi/T_{n,0}$, where $T_{n,0}$ is the initial fundamental period of the rocking system (Eq. (11)). Although both choices are admittedly quite arbitrary, according to initial sensitivity analyses, the performance of the simplified model is insensitive to the values of $K_{H,}$ C_H, $K_{V,}$ and C_V – at least for the relatively slender systems considered herein.

The SDOF system is initially subjected to artificial sinusoidal excitations, to check the effectiveness of the proposed methodology under idealized conditions, and then to real moderate to strong intensity seismic records of (Fig. 11). Before proceeding to the comparisons, the results of initial sensitivity analyses are briefly discussed.

7.1. Sensitivity with respect to C_R

Recognizing that most commercial FE codes do not accept nonlinear dashpots, in order to maintain simplicity a linear dashpot is considered. Within this realm, a simplifying approximation is proposed, assuming the maximum value of the normalized C_R–θ curves of Fig. 7d. Moreover, the damping coefficient C_R also depends on the angular frequency $\omega=2\pi/T$, and since the effective period T_n of the rocking system is a function of rotation, an additional simplifying approximation has been proposed, using the initial natural period $T_{n,0}$ of the rocking system (Eq. (11)) to compute C_R. In this section, the validity of these approximations is tested through sensitivity analysis with respect to the damping coefficient C_R.

With respect to ω, two radically different assumptions are comparatively assessed: (a) the proposed initial natural frequency of the rocking system $\omega_n=2\pi/T_n$ ($=2\pi/0.39$ s$=16.1$ rad/s); and (b) the predominant frequency of the seismic excitation $\omega_p=2\pi/T_p$. To make a strong point, the Lucerne(000) record from the 1992 M_S 7.3 Landers earthquake is used as seismic excitation. Characterized by a high frequency content, its predominant frequency $\omega_p=2\pi/0.08=78.5$ rad/s, is much larger than ω_n. The 3D FE model is used as a yardstick to infer on the comparative efficiency of the two assumptions. Fig. 12a compares the two different assumptions with respect to ω, in terms of rotation time histories for a SDOF system with $F_S=3.3$. When the initial natural frequency of the rocking system ω_n is used to compute the damping coefficient C_R, the simplified model captures the rotation time history with remarkable accuracy. When the predominant frequency of the seismic excitation ω_p is used, the performance of the simplified model becomes much worse. Note that the two different assumptions with respect to ω yield rotational damping coefficients having a difference of the order of 5 (since $\omega_p/\omega_n \approx 5$), and, hence, the observed differences are quite reasonable. Evidently, the ω_p assumption leads to substantial underestimation of C_R.

With respect to the assumption of the maximum value of the normalized C_R–θ curves, three alternatives are tested: (a) the proposed maximum value of the normalized C_R–θ curves, denoted hereafter $C_{R,max}$; (b) a somehow reduced value of $0.75C_{R,max}$; and (c) a drastically reduced value of $0.25C_{R,max}$. Fig. 12b compares the three different assumptions, in terms of rotation time histories for a SDOF system with $F_S=2.5$ subjected to a moderate intensity seismic record, from the 1986 M_S 6 Kalamata (Greece) earthquake (keeping the value of $\omega=\omega_n$ constant). When considering $0.25C_{R,max}$, the simplified model fails to reproduce the rotation time history of the more rigorous 3D FE model: damping is considerably underestimated, leading to unrealistic response. On the contrary, the discrepancies between the $0.75C_{R,max}$ and $C_{R,max}$ assumptions are not that pronounced, implying that the problem is not so sensitive to the exact value of C_R: if the order of magnitude is correct, the prediction of the simplified model should be reasonably accurate. The optimum result is obtained for $C_{R,max}$, in which case the simplified model captures the performance quite precisely.

7.2. Moderate seismic shaking

The performance of the simplified model is initially evaluated for moderate intensity seismic motions. Two such examples are presented in Fig. 13, referring to a system of height $h=4$ m, mass $m=75$ Mgr, and $F_s=2.5$ subjected to an idealized artificial Tsang-type seismic excitation, and the El Centro (180) record from the 1940 M_S 6.9 Imperial Valley earthquake. Both seismic excitations contain multiple strong motion cycles of moderate amplitude (0.3 g to 0.4 g), encompassing the characteristics of far-field multi-cycle seismic motions.

The Tsang-type excitation is *symmetric*, containing a multitude of strong motion cycles of amplitude $a_E=0.4$ g at predominant frequency $f_E=2$ Hz. The numerical prediction of the simplified model is compared to the more rigorous 3D FE model in terms of

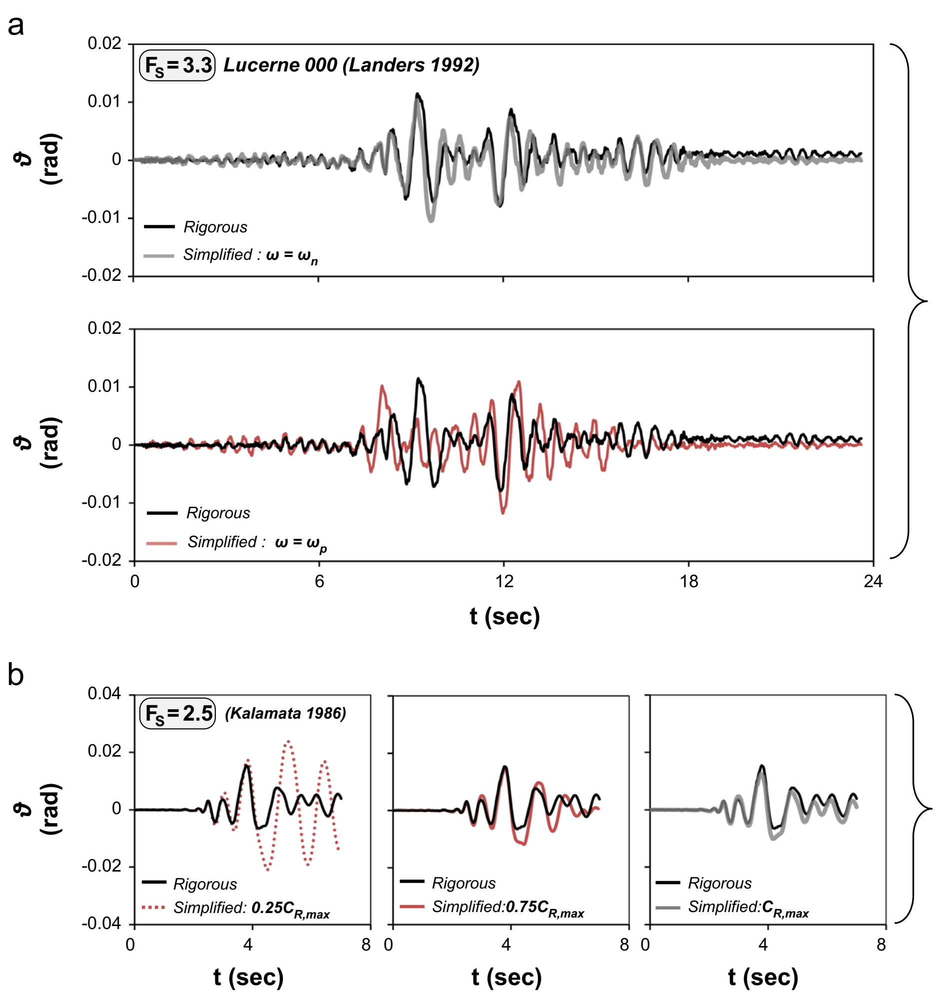

Fig. 12. Sensitivity analysis with respect to C_R: (a) comparison of two different assumptions with respect to the angular frequency ω for a system having $F_S=3.3$, subjected to the Lucerne(000) record; and (b) comparison of three different assumptions with respect to the maximum value of C_R for a system having $F_S=2.5$, subjected to the Kalamata 1986 record.

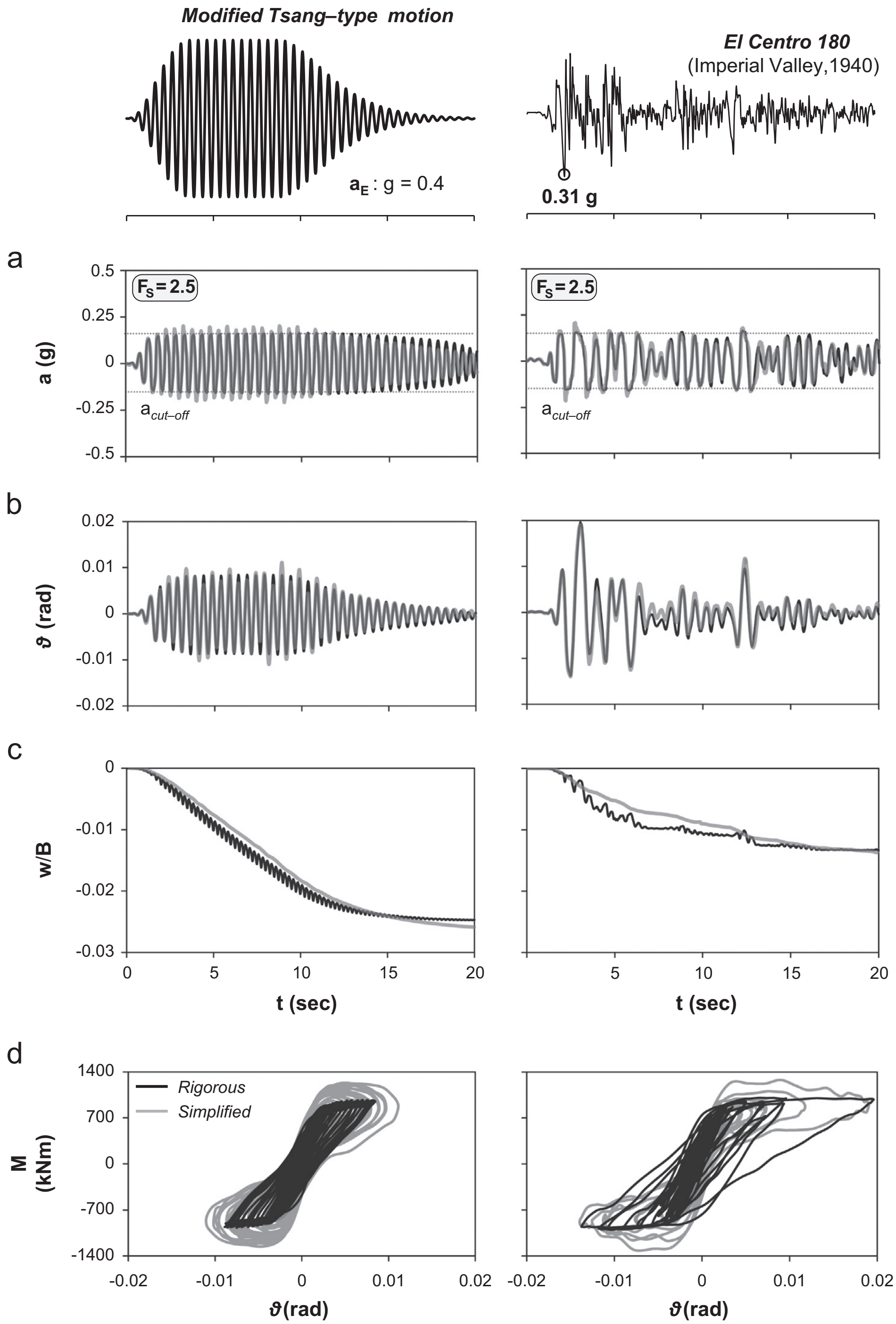

Fig. 13. Effectiveness of the simplified method for moderate intensity seismic shaking. Comparison of the numerical prediction of the simplified model with the results of the rigorous 3D FE model, for a system with F_S=2.5 subjected to an artificial Tsang-Type motion (left column) and the El Centro(180) record (right column). Time histories of: (a) acceleration at the oscillator, (b) foundation rotation, and (c) foundation settlement; (d) moment–rotation (M–θ) loops at the foundation level.

time histories of acceleration at the oscillator mass, foundation rotation, and settlement, as well as moment–rotation (M–θ) loops at the foundation level. As shown in Fig. 13a and b (left column), the simplified model captures the acceleration and foundation rotation time histories with remarkable accuracy: the predicted time histories are practically identical to those of the 3D FE model. It is worth noting that the maximum acceleration at the oscillator mass is significantly lower than the peak acceleration of the seismic excitation (a_E=0.4 g), revealing that the foundation has reached its moment capacity, responding in the nonlinear range. Due to the relatively low factor of safety F_S=2.5, extensive soil yielding takes place underneath the foundation, limiting the inertia transmitted onto the superstructure. As depicted in Fig. 13c (left column), the estimation of the (normalized with B) dynamic settlement using the previously described simplified procedure (on the basis of the time history of θ, as predicted by the simplified model) is equally successful. In terms of the M–θ loops (Fig. 13d), the comparison is also acceptable, with the simplified model having a tendency to overestimate the moment and the rotation, but capturing the shape of the loop quite nicely. This difference is due to the previously discussed approximations with respect to the rotational dashpot.

The El Centro (180) record is selected for two reasons: (i) having a PGA=0.31 g, and containing a multitude of strong motion cycles of various frequencies, it may be considered representative of a typical design earthquake, at least in terms of spectral acceleration (see Fig. 11); and (ii) being a far-field record, it is not affected by forward-rupture directivity effects, which tend to complicate the response of strongly nonlinear systems, such as the one investigated herein. As shown in Fig. 13a–c (right column), the simplified model captures the acceleration, rotation, and settlement time histories quite nicely. The latter cannot possibly be reproduced in detail, as the simplified procedure does not account for the uplifting *during* each half-cycle of loading. Finally, the comparison is also quite successful in terms of M–θ loops (Fig. 13d). Observe that the real record, despite having a lower PGA (0.31 g as opposed to 0.4 g of the Tsang-type motion), leads to the development of larger foundation rotation θ and increased soil inelasticity. On the other hand, due to its multitude of strong motion cycles (of constant amplitude a_E=0.4 g), the Tsang-type excitation produces substantially larger dynamic settlement.

7.3. Strong seismic shaking

The efficiency of the simplified method is explored further, focusing on strong (to very strong) seismic motions, during which the response of the rocking system is expected to be highly nonlinear. A characteristic example is presented in Fig. 14, utilizing

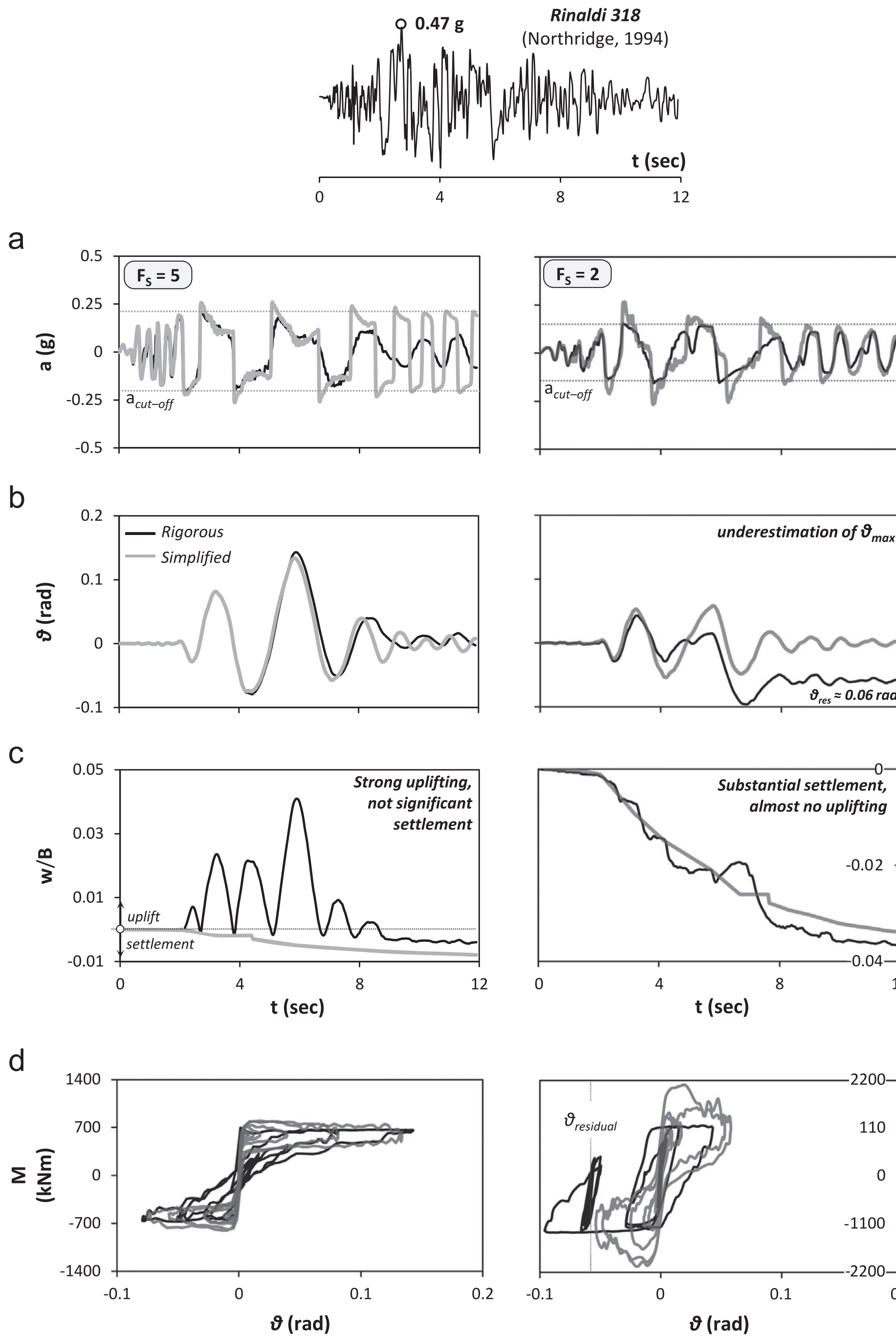

Fig. 14. Effectiveness of the simplified method for strong seismic shaking, using the Rinaldi (318) record as seismic excitation. Comparison of the numerical prediction of the simplified model with the results of the rigorous 3D FE model, for two different factors of safety: F_S=5 (left column) and F_S=2 (right column). Time histories of: (a) acceleration at the oscillator, (b) foundation rotation, and (c) foundation settlement; (d) moment–rotation (M–θ) loops at the foundation level.

the Rinaldi (318) record from the 1994 M_S 7.2 Northridge as seismic excitation. The latter is a particularly destructive near-field record, encompassing the effects of forward-rupture directivity. Two different factors of safety are investigated, one being representative of (relatively) lightly-loaded systems, $F_S=5$ (left column), and the other referring to more heavily-loaded systems, $F_S=2$ (right column).

As evidenced by the acceleration time histories of Fig. 14a, the Rinaldi record is, indeed, quite extreme for the lightly-loaded $F_S=5$ system. Observe the acceleration cut-off at roughly 0.24 g (corresponding to the critical acceleration of the rocking system), which is repeatedly of particularly long-duration. During each acceleration "plateau", the foundation reaches its moment capacity, exhibiting strongly-nonlinear response. Limiting the inertia transmitted to the superstructure, this acceleration cut-off is obviously advantageous. As a result, however, the system is forced to excessively large rotations of the order of 0.1 rad (Fig. 14b) – almost an order of magnitude larger compared to the previous cases. The simplified model captures correctly the acceleration cut-off, being less accurate in terms of the details of the acceleration time history. Interestingly, despite these discrepancies, the rotation time history is predicted with impressive accuracy (minor discrepancies can be observed only towards the end). Although the footing develops large rotations, the residual rotation at the end of shaking is practically negligible: an inherent self-centering attribute of rocking systems, provided that the factor of safety against vertical loading is adequately large ($F_s \geq 5$ for clay), so as to ensure uplifting-dominated response. As shown in Fig. 14c, the residual settlement is slightly overestimated, being, however, almost negligible thanks to the uplifting-dominated response of the system. As previously discussed, the simplified approximate settlement–rotation relations of Eq. (12) are conservative, especially for large F_s (see Fig. 9). Hence, this difference is quite natural. Moreover, the upward displacement due to uplifting cannot possibly be captured by the simplified method. Finally, the comparison is excellent in terms of moment–rotation (M–θ) loops (Fig. 14d).

In the case of the heavily-loaded $F_S=2$ system (right column of Fig. 14), the discrepancies between the simplified and the 3D FE model are far more pronounced. Although the simplified model does capture the moment capacity of the system, as evidenced by the acceleration cut-off in Fig. 14b, due to the very low F_S excessive plastic deformation takes place during strong seismic shaking leading to the development of very large irrecoverable rotations (Fig. 14b). As a result, the residual rotation $\theta_{res} \approx 0.06$ rad is not at all negligible, and cannot possibly be captured by the simplified model. Quite surprisingly, the total prediction of the dynamic settlement is satisfactory (Fig. 14c). Although this might seem as a paradox, it is quite easily explainable. With the exception of rotation accumulation, the rotation time history is not poorly predicted, at least with respect to the amplitude of individual rotation half-cycles. Consequently, there is no reason for the settlement not to be predicted correctly. The M–θ loops of Fig. 14d confirm the yielding-dominated behavior of the system, and the (natural and expected) inability of the simplified model to capture the residual rotation. Most importantly, in this case the

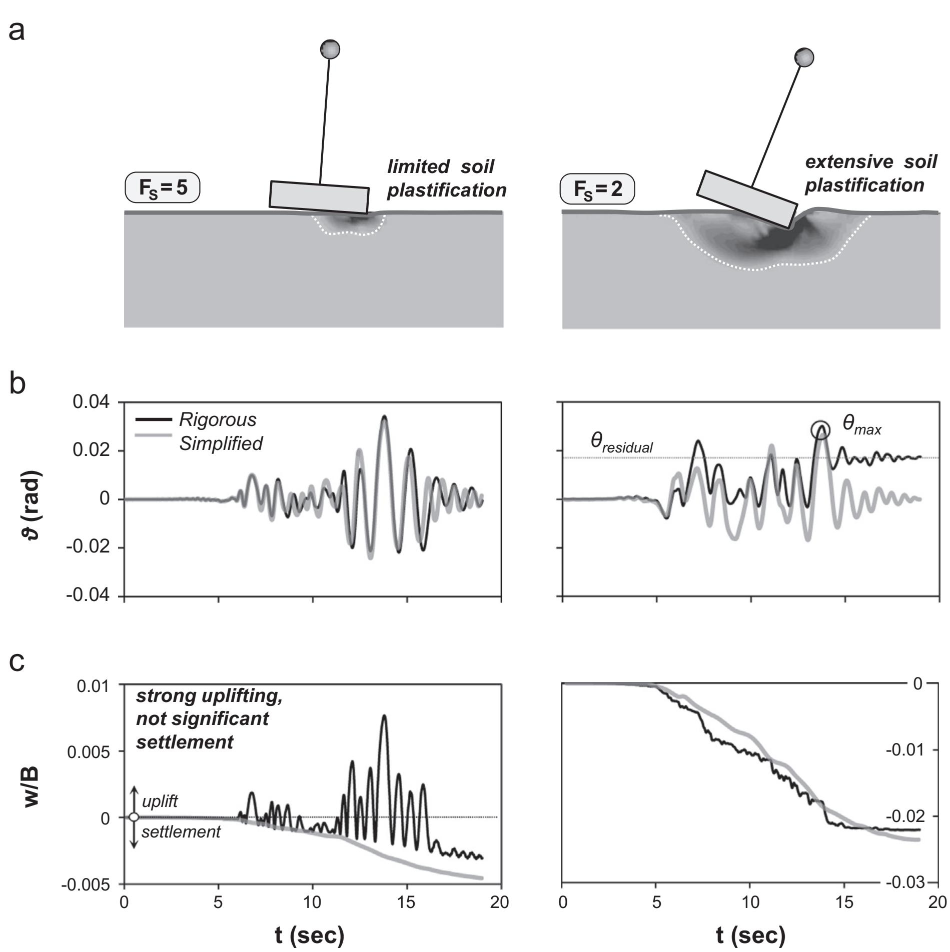

Fig. 15. Effectiveness of the simplified method for strong seismic shaking, using the Yarimca (060) record as seismic excitation. Comparison of the numerical prediction of the simplified model with the results of the rigorous 3D FE model, for two different factors of safety: $F_S=5$ (let column) and $F_S=2$ (right column): (a) deformed mesh with plastic strain contours (rigorous model); time histories of (b) foundation rotation, and (c) settlement.

simplified model substantially overestimates the developing moment. This is directly related to the linear dashpot, which is connected in parallel with the nonlinear rotational spring. It is a clear shortcoming of the simplified method, which is, however, of importance for low factors of safety F_S combined with very strong directivity-affected seismic excitations. In such cases, the simplified model should be used with caution, as the error in predicting the inertia loading of the system can be quite substantial. The problem can be solved by connecting the spring in series, as described by Wang et al. [60].

It should be emphasized, however, that the previous example is actually a worst-case scenario, not being representative of the overall performance of the simplified method. In general, even for very low F_S and seismic motions containing strong directivity pulses, its performance is on average quite acceptable. Actually, in the majority of the cases examined the accumulation of residual rotation does not seem to affect the estimation of maximum rotation, which is of prime significance for design purposes. One such example is given in Fig. 15, referring to the same factors of safety (F_S=5 and 2), but using as seismic excitation the Yarimca (060) record from the 1999 M_S 7.4 Kocaeli earthquake. The two snapshots of deformed mesh with superimposed plastic strain contours (computed with the more rigorous 3D FE model) at the end of seismic shaking (Fig. 15a) show vividly the fundamental difference in the response of the two systems. While for F_S=5 the behavior is clearly uplifting-dominated, with plastic deformation being localized within a very narrow zone underneath the foundation, the performance of the F_S=2 system is characterized by extensive soil plastification. As expected, for the lightly-loaded (F_S=5) system the simplified method predicts the time history of rotation quite accurately (Fig. 15b). But even for the heavily-loaded (F_S=2) system, although the rotation time histories do not perfectly match (due to the unavoidable accumulation of rotation), the maximum value of θ is predicted quite successfully. As for the previous example, the simplified method captures the settlement with remarkable accuracy (Fig. 15c). Despite the above mentioned problems, the simplified method seems to perform better for the heavily-loaded system, overestimating the settlement of the lightly-loaded one. This is directly associated to the conservatism of the proposed Δw–θ relations (see Eq. (12)).

8. Synopsis and conclusions

This paper has introduced a simplified method to analyze the seismic performance of rocking systems, taking account of soil inelasticity and foundation uplifting. The soil–foundation system is replaced by springs and dashpots. While the horizontal (K_H and C_H) and vertical (K_V and C_V) springs and dashpots are assumed elastic, directly obtained by published solutions [21], for the rotational degree of freedom a *nonlinear rotational spring* is employed, accompanied by a *linear dashpot*. Three relations are required, all of them being a function of the factor of safety against vertical loading F_S: (a) the moment–rotation (M–θ) relation, (b) the damping coefficient–rotation (C_R–θ) relation, and (c) the dynamic settlement–rotation (Δw_{dyn}–θ) relation. Focusing on square shallow foundations, the necessary relations are computed through 3D FE analyses, applying a thoroughly validated constitutive model [4].

The effectiveness of the proposed simplified method has been demonstrated through comparisons with 3D FE analyses. Fig. 16 summarizes the performance of the simplified method for all seismic excitations examined, and for three different factors of safety against vertical loading F_S=5, 3.3, and 2. The comparison is performed in terms of maximum rotation θ_{max} and dimensionless

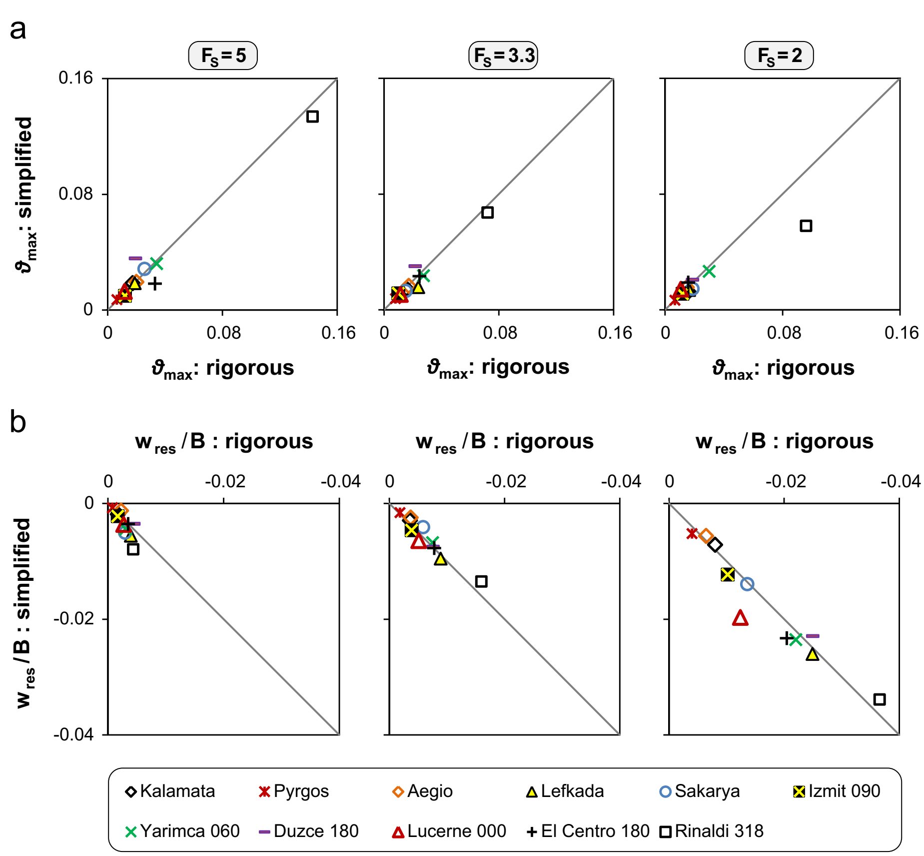

Fig. 16. Comparative summary for all seismic records examined, and factors of safety F_S=5, 3.3, and 2: (a) maximum rotation θ_{max} predicted by the simplified model compared to the rigorous model; and (b) normalized residual settlement w_{res}/B predicted by the simplified model compared to the rigorous model.

residual settlement w_{res}/B, plotting the prediction of the simplified model (vertical axis) against the corresponding results of the rigorous 3D FE model (horizontal axis). At least for the cases examined, the effectiveness of the simplified method is fully confirmed. In terms of θ_{max} (Fig. 16a), its effectiveness is quite impressive for all factors of safety. The only substantial discrepancy is observed for the heavily-loaded ($F_S=2$) system subjected to the directivity-affected Rinaldi record. This is related to the inability of the simplified model to capture residual rotations – an unavoidable shortcoming, which is, however, of importance mainly for (unrealistically) low F_S combined with very strong seismic shaking with directivity-affected seismic excitations. The residual settlement is accurately predicted for all cases examined (Fig. 16b).

Although the proposed simplified method is based on several simplifying approximations (some of them being, admittedly, quite crude), it is considered as a valid alternative for the preliminary design of rocking-isolated systems. Being easily implementable in commercial FE codes, without requiring calibration of sophisticated models and avoiding the need for time consuming 3D FE analyses, it has the potential of being applied in practice in the near future. The proposed procedure is simple and straightforward, not requiring iterations to compute the response. Although this paper has focused on square foundations, the same methodology can be employed for other footing shapes (rectangular, circular, strip), or for embedded foundations. Alternatively, the required relations can be produced *experimentally*, on the basis of cyclic pushover tests (e.g., [40,18,5,6]). Hence, the practicing engineer may directly apply the proposed methodology utilizing the provided FE-derived relations, or select from the literature other relations that may be considered more appropriate.

Acknowledgment

The financial support for this paper has been provided under the research project “DARE”, which is funded through the European Research Council's (ERC) “IDEAS” Programme, in Support of Frontier Research-Advanced Grant, under contract/number ERC-2-9-AdG228254-DARE to Prof. G. Gazetas.

References

[1] Allotey N, El Naggar MH. An investigation into the Winkler modeling of the cyclic response of rigid footings. Soil Dynamics and Earthquake Engineering 2007;28:44–57.
[2] Anastasopoulos I. Beyond conventional capacity design: towards a new design philosophy. In: Orense RP, Chouw N, Pender MJ, editors. Soil–Foundation–Structure Interaction. New York: CRC Press, Taylor & Francis Group; 2010.
[3] Anastasopoulos I, Gazetas G, Loli M, Apostolou M, Gerolymos N. Soil failure can be used for seismic protection of structures. Bulletin of Earthquake Engineering 2010;8:309–26.
[4] Anastasopoulos I, Gelagoti F, Kourkoulis R, Gazetas G. Simplified Constitutive model for simulation of cyclic response of shallow foundations: validation against laboratory tests. Journal of Geotechnical and Geoenvironmental Engineering, ASCE 2011;137(12)1154–68.
[5] Anastasopoulos I, Kourkoulis R, Gelagoti F, Papadopoulos E. Metaplastic rocking response of SDOF systems on shallow improved sand: an experimental study. Soil Dynamics and Earthquake Engineering 2012;40:15–33.
[6] Anastasopoulos I, Loli M, Gelagoti F, Kourkoulis R, Gazetas G. Nonlinear soil–foundation interaction: numerical analysis. In: Proceedings of the 2nd international conference on performance-based design in earthquake geotechnical engineering. Taormina, Italy, May 28–30; 2012b.
[7] Anastasopoulos I, Gelagoti F, Spyridaki A, Sideri Tz, Gazetas G. Seismic rocking isolation of asymmetric frame on spread footings. Journal of Geotechnical and Geoenvironmental Engineering, ASCE 2014;140(1). http://dx.doi.org/10.1061/(ASCE)GT.1943-5606.0001012.
[8] Apostolou M, Gazetas G. Analytical modelling of footings under large overturning moment. In: Proceedings of the 2nd Japan–Greece workshop on seismic design, observation, retrofit of foundations. Tokyo, Japan; 2007. p. 165–184.
[9] Bienen B, Gaudin C, Cassidy MJ. Centrifuge tests of shallow footing behavior on sand under combined vertical-torsional loading. International Journal of Physical Modelling in Geotechnics 2007;2:1–21.
[10] Bransby MF, Randolph MF. Combined loading of skirted foundations. Géotechnique 1998;48(5):637–55.
[11] Butterfield R, Gottardi G. A complete three-dimensional failure envelope for shallow footings on sand. Géotechnique 1994;44(1):181–4.
[12] Chatzigogos CT, Pecker A, Salençon J. Macroelement modeling of shallow foundations. Soil Dynamics and Earthquake Engineering 2009;29(5):765–81.
[13] Crémer C, Pecker A, Davenne L. Cyclic macro-element for soil–structure interaction: material and geometrical nonlinearities. International Journal for Numerical and Analytical methods in Geomechanics 2001;25(12):1257–84.
[14] Deng L, Kutter BL, Kunnath SK. Centrifuge modeling of bridge systems designed for rocking foundations. Journal of Geotechnical and Geoenvironmental Engineering 2012;138(3):335–44.
[15] Faccioli E, Paolucci R, Vanini M, editors. TRISEE: 3D site effects and soil–foundation interaction in earthquake and vibration risk evaluation. European Commission Publications; 1999.
[16] Figini R, Paolucci R, Chatzigogos CT. A macro-element model for non-linear soil–shallow foundation–structure interaction under seismic loads: theoretical development and experimental validation on large scale tests. Earthquake Engineering and Structural Dynamics 2012;41:475–93.
[17] Furumura T, Takemura S, Noguchi S, Takemoto T, Maeda T, Iwai K, et al. Strong ground motions from the 2011 off-the-Pacific-Coast-of-Tohoku, Japan (Mw=9.0) earthquake obtained from a dense nationwide seismic network. Landslides 2011;8(3):333–8.
[18] Gajan S, Phalen JD, Kutter BL, Hutchinson TC, Martin G. Centrifuge modeling of load deformation behavior of rocking shallow foundations. Soil Dynamics and Earthquake Engineering 2005;25(7–10):773–83.
[19] Gajan S, Kutter BL. Capacity, settlement and energy dissipation of shallow footings subjected to rocking. Journal of Geotechnical and Geoenvironmental Engineering, ASCE 2008;134(8)1129–41.
[20] Gajan S, Kutter BL. Effects of moment-to-shear ratio on combined cyclic load–displacement behavior of shallow foundations from centrifuge experiments. Journal of Geotechnical and Geoenvironmental Engineering, ASCE 2009;135(8)1044–55.
[21] Gazetas G. Analysis of machine foundation vibrations: state of the art. Soil Dynamics and Earthquake Engineering 1983;2:2–42.
[22] Gazetas G. Formulas and charts for impedances of surface and embedded foundations. Journal of Geotechnical Engineering, ASCE 1991;117(9)1363–81.
[23] Gazetas G, Apostolou M. Nonlinear soil–structure interaction: foundation uplifting and soil yielding. In: Proceedings 3rd UJNR workshop on soil–structure interaction. Menlo Park, California, USA (CD-ROM); 2004.
[24] Gazetas G, Apostolou M, Anastasopoulos I. Seismic uplifting of foundations on soft soil, with examples from Adapazari (Izmit 1999, Earthquake). BGA international conference of foundations: innovations, observations, design and practice. Scotland: University of Dundee; 2003; 37–50.
[25] Gazetas G, Anastasopoulos I, Adamidis O, Kontoroupi T. Nonlinear rocking stiffness of foundations. Soil Dynamics and Earthquake Engineering 2013;47:83–91.
[26] Gelagoti F, Kourkoulis R, Anastasopoulos I, Gazetas G. Seismic wave propagation in Alluvial Valleys: sensitivity to ground motion details and soil nonlinearity, generation of parasitic vertical component. Bulletin of the Seismological Society of America 2010;100(6):3035–54.
[27] Gelagoti F, Kourkoulis R, Anastasopoulos I, Gazetas G. Rocking isolation of low rise frame structures founded on separate footings. Earthquake Engineering and Structural Dynamics 2012;41:1177–97.
[28] Gelagoti F, Kourkoulis R, Anastasopoulos I, Gazetas G. Rocking-isolated frame structures: margins of safety against toppling collapse and simplified design approach. Soil Dynamics and Earthquake Engineering 2012;32(1):87–102.
[29] Gerolymos N, Gazetas G. Seismic response of yielding pile in non-linear soil. In: Proceedings of the 1st Greece–Japan workshop on seismic design, observation, retrofit of foundations. Athens, Greece; 2005. p. 25–37.
[30] Gourvenec S. Shape effects on the capacity of rectangular footings under general loading. Géotechnique 2007;57(8):637–46.
[31] Gourvenec S, Randolph MF. Effect of strength non-homogeneity on the shape and failure envelopes for combined loading of strip and circular foundations on clay. Géotechnique 2003;53(6):527–33.
[32] Harden C, Hutchinson T. Investigation into the effects of foundation uplift on simplified seismic design procedures. Earthquake Spectra 2006;22(3):663–92.
[33] Houlsby GT, Amorosi A, Rojas E. Elastic moduli of soils dependent on pressure: a hyperelastic formulation. Géotechnique 2005;55(5):383–92.
[34] Housner GW. The behaviour of inverted pendulum structures during earthquake. Bulletin of the Seismological Society of America 1963;53(2):403–17.
[35] Jennings PC, Bielak J. Dynamics of building–soil interaction. Bulletin of the Seismological Society of America 1973;63(1):9–48.
[36] Kausel E, Roesset JM. Dynamic stiffness of circular foundations. Journal of Engineering Mechanics Division, ASCE 1975771–85.
[37] Knappett JA, Haigh SK, Madabhushi SPG. Mechanisms of failure for shallow foundations under earthquake loading. Soil Dynamics and Earthquake Engineering 2006;26:91–102.
[38] Kourkoulis R, Anastasopoulos I, Gelagoti F, Kokkali P. Dimensional analysis of SDOF system rocking on inelastic soil. Journal of Earthquake Engineering 2012;16:995–1022.
[39] Kourkoulis R, Gelagoti F, Anastasopoulos I. Rocking isolation of frames on isolated footings: design insights and limitations. Journal of Earthquake Engineering 2012;16(3):374–400.
[40] Kutter BL, Martin G, Hutchinson TC, Harden C, Gajan S, Phalen JD. Status report on study of modeling of nonlinear cyclic load–deformation behavior of

shallow foundations. University of California, Davis, Proceedings of the PEER Workshop; 2003.

[41] Kutter BL, Wilson DL. Physical modeling of dynamic behavior of soil–foundation–superstructure systems. International Journal of Physical Modeling in Geotechnics 2006;6(1):1–12.

[42] Kutter et al., Estimation of displacement demand for seismic design of bridges with rocking shallow foundations. In: Proceedings of the 5th International conference on recent advances in geotechnical earthquqke engineering and soil dynamics, San Diego; 2010.

[43] Le Pape Y, Sieffert JP. Application of thermodynamics to the global modeling of shallow foundations on frictional material. International Journal for Numerical and Analytical Methods in Geomechanics 2001;25:1377–408.

[44] Martin CM, Houlsby GT. Combined loading of spudcan foundations on clay: numerical modeling. Géotechnique 2001;51(8):687–99.

[45] Maugeri M, Musumeci G, Novità D, Taylor CA. Shaking table test of failure of a shallow foundation subjected to an eccentric load. Soil Dynamics and Earthquake Engineering 2000;20(5–8):435–44.

[46] Mergos PE, Kawashima K. Rocking isolation of a typical bridge pier on spread foundation. Journal of Earthquake Engineering 2005;9(2):395–414.

[47] Meyerhof GG. The bearing capacity of foundations under eccentric and inclined loads. In: Proceedings of the 3rd international conference of soil mechanics and foundation engineering, Zurich, vol. 1; 1953. p. 440–445.

[48] Negro P, Paolucci R, Pedretti S, Faccioli E. Large scale soil–structure interaction experiments on sand under cyclic load. In: Proceedings of 12th world conference on earthquake engineering, Paper no. 1191, Auckland, New Zealand; 2000.

[49] Nova R, Montrasio L. Settlement of shallow foundations on sand. Géotechnique 1991;41(2):243–56.

[50] Paolucci R. Simplified evaluation of earthquake induced permanent displacements of shallow foundations. Journal of Earthquake Engineering 1997;1:563–79.

[51] Paolucci R, Shirato M, Yilmaz MT. Seismic behavior of shallow foundations: shaking table experiments vs. numerical modeling. Earthquake Engineering & Structural Dynamic 2008;37(4):577–95.

[52] Paolucci R, Figini R, di Prisco C, Petrini L, Vecchiotti M. Accounting for nonlinear dynamic soil–structure interaction in the displacement-based seismic design. In: Proceedings of the 5th international conference on earthquake geotechnical engineering. Santiago, Chile (CD-ROM); 2011.

[53] Pecker A. A seismic foundation design process, lessons learned from two major projects: the Vasco de Gama and the Rion Antirion bridges. ACI International Conference on Seismic Bridge Design and Retrofit. La Jolla, USA: University of California at San Diego; 2003.

[54] Pender M. Seismic design and performance of surface foundations. In: Proceedings of the 4th international conference on earthquake geotechnical engineering, Thessaloniki, Greece (CD-ROM); 2007.

[55] Priestley MJN, Calvi GM, Kowalski MJ. Displacement based seismic design of structures. Pavia: IUSS press; 2007.

[56] Raychowdhury P, Hutchinson T. Performance evaluation of a nonlinear Winkler-based shallow foundation model using centrifuge test results. Earthquake Engineering and Structural Dynamics 2009;38(5):679–98.

[57] Tassoulas JL. An investigation of the effect of rigid sidewalls on the response of embedded circular foundations to obliquely-incident SV and P waves. Dynamic Soil–Structure Interaction. Rotterdam: A.A.Balkemal; 1984; 55–63.

[58] Ukritchon B, Whittle AJ, Sloan SW. Undrained limit analysis for combined loading of strip footings on clay. Journal of Geotechnical and Geoenvironmental Engineering, ASCE 1998;124(3)265–76.

[59] Veletsos AS, Nair VV. Seismic interaction of structures on hysteretic foundations. Journal of Structural Engineering, ASCE 1975;101(1)109–29.

[60] Wang S, Kutter BL, Chacko MJ, Wilson DW, Boulanger RW, Abghari A. Nonlinear seismic soil–pile structure interaction. Earthquake Spectra 1998;14(2):377–96.

[61] Wong HL, Luco JE. Tables of impedance functions for square foundations on layered media. Soil Dynamics and Earthquake Engineering 1985;4:64–81.